AIP | Journal of Applied Physics

Computer simulation and experimental study of elastic properties of amorphous Cu-Zr alloys

M. I. Mendelev, D. K. Rehbein, R. T. Ott, M. J. Kramer, and D. J. Sordelet

Citation: J. Appl. Phys. **102**, 093518 (2007); doi: 10.1063/1.2805655
View online: http://dx.doi.org/10.1063/1.2805655
View Table of Contents: http://jap.aip.org/resource/1/JAPIAU/v102/i9
Published by the American Institute of Physics.

Computer simulation and experimental study of elastic properties of amorphous Cu-Zr alloys

M. I. Mendelev,[a] D. K. Rehbein, R. T. Ott, M. J. Kramer, and D. J. Sordelet
Materials and Engineering Physics Program, Ames Laboratory, Ames, Iowa 50011, USA

(Received 22 June 2007; accepted 12 September 2007; published online 13 November 2007)

Molecular-dynamics simulations were performed to determine the elastic constants of Cu_xZr_{100-x} $(33.3 \leq x \leq 64.5)$ metallic glasses at room temperature. The accuracy of the interatomic potentials used to obtain the model glass structures was tested by comparing to the total structure factors obtained from high-energy synchrotron x-ray diffraction and, more importantly, to acoustic velocities measured from melt spun ribbons. Both the simulated and measured acoustic velocities increased at comparable rates with increasing Cu concentration, but the former underestimated the latter by about 10%. Young's moduli of the simulated models were determined by combining the ultrasonic data with densities that were obtained from simulations. In addition, the compositional dependence of Poisson's ratio, shear modulus, and bulk modulus for this series of simulated metallic glasses was determined. Examination of partial-pair correlations deduced from simulated glass structures shows a correlation between higher bulk moduli in Cu-rich compositions and concomitant changes in Zr-Zr nearest neighbors, which exhibit a stronger sensitivity to an imposed hydrostatic stress than do Cu-Cu or Cu-Zr nearest-neighbor distances. © *2007 American Institute of Physics*. [DOI: 10.1063/1.2805655]

I. INTRODUCTION

Determining the elastic constants of metallic glasses has both practical and fundamental relevance. The former is linked, for example, to finding new materials having higher stiffness for a given density. The latter connection has received considerable attention recently as a corollary to help understand the expanding contrast in deformation behavior among the rapidly growing list of alloys that can form a metallic glass. In addition, there is speculation that the temperature dependence of the shear modulus has been directly related to the viscosity and hence fragility that may contribute to glass formability, but this has been disputed.[1,2] In particular, the ratio of the elastic shear modulus, μ, to the bulk modulus, B, has been used as a parameter to compare the tendency for brittle behavior versus the capacity to exhibit room-temperature ductility. As clearly described in Refs. 3 and 4, metallic glasses showing plasticity should not be termed globally ductile, but instead should be considered to be malleable since they are capable of plastic compression and may be bent plastically. In this light, a wide range of μ/B values have been determined for different metallic glasses that exhibit markedly contrasting deformation tendencies. For example, at Pt-based metallic glass that has been shown to exhibit plastic strain to failure in compression approaching 20% has a μ/B value of 0.165,[5] while in contrast a Mg-based metallic glass that shows almost no plastic strain in compression has a much higher μ/B value of 0.439.

A recent comprehensive survey of the correlation between elastic moduli and the mechanical behavior of metallic glasses helps to illustrate the wide breadth of properties and deformation characteristics among materials that all have in common the absence of long-range atomic order.[6–9] In addition, others have proposed using elastic constants as a way to gain additional insight into the static structure and dynamic thermal response of metallic glass. Rouxel[10] reviewed the variation in elastic properties of amorphous materials, including some metallic glasses, having varying short- and medium-range ordering. Wang[11] surveyed available dynamic fragility data among many metallic glasses in order to search for a connection to their elastic constants. Collectively, these reports as well as other related literature help to demonstrate the importance of both determining the elastic constants of specific metallic glasses and understanding their correlation to glass structure and dynamic behavior.

While some mechanical properties of metallic glasses may be determined relatively easily from experiments, it is a much more complicated task to obtain associated information at the atomic level from experiments. It is possible, however, to extract such information from atomistic computer simulations. Since the metallic glass structure is inherently nonsymmetric, simulations frequently require using large models (i.e., more than several thousand atoms) that should be relaxed during rather long times to reach at least some equilibrium state, which precludes the application of first-principles methods. While the structure of a metallic glass can be modeled without *a priori* knowledge of interatomic interactions based on data from diffraction experiments (e.g., see Refs. 12–15), these methods do not allow us to either reliably calculate the mechanical properties or to study any dynamic atomic transport processes. As a consequence, using the semiempirical potential appears to be the most reasonable option for simultaneously studying both the structure and mechanical properties of metallic glasses.

The simplest type of semiempirical potentials is a pair potential (including hard-sphere potentials as the simplest

[a]Author to whom correspondence should be addressed: mendelev@ameslab.gov

possible approximation). These potentials were widely used in earlier molecular-dynamics (MD) simulations (e.g., see Refs. 16–20) and these studies definitely enriched our knowledge about the structure and mechanical properties of metallic glasses. However, the reports by Daw and Baskes[21] and Finnis and Sinclair,[22] who proposed new types of many-body potentials for metallic systems, make it clearly sensible to use these potentials if the primary goal is not to gain just qualitative information, but rather to compare with real experimental data. The point is that pair potentials in principle cannot describe some important crystalline metal properties, including the nonzero difference between cohesive and unrelaxed vacancy formation energies and the Cauchy pressure. The latter deficiency can be especially crucial if the potentials are employed to study mechanical properties. Taking into account that the many-body potentials proposed in Refs. 21 and 22 are capable of fixing this problem and, furthermore, require about the same computational time as pair potentials, the use of these types of semiempirical potentials to simulate the properties of metallic glasses appears to be very reasonable.

Obviously, the results of atomistic computer simulations depend strongly on the quality of the employed semiempirical potential. Therefore, it is a good idea to test a particular potential by comparison of simulated results to the experimental data that are relevant to the problem that will be investigated using this potential. The goal of the present study is to apply the semiempirical potential proposed for Cu-Zr metallic glasses in Ref. 23 for determining the elastic constants of the Cu-Zr metallic glasses and compare selected quantities to those determined by independent experimental techniques. It should be noted that elastic constants for Cu-Zr metallic glasses were already determined in Ref. 18. However, the authors of that work used a pair potential in their simulations, which may not be well justified according to the discussion presented earlier. Moreover, while the authors of Ref. 18 focused on the dependence of the elastic constants on the free volume, a corollary dependence of these properties on composition was not established.

The remainder of this paper is organized as follows. In the next section, we present the results of the experimental determination of the acoustic velocity in amorphous Cu_xZr_{100-x} $(33.3 \leq x \leq 64.5)$ alloys. Then we present the results of the MD calculations of the same property for the same compositions. As will be discussed, good agreement was found between experimental and simulation data, thus allowing us to trust elastic constants found in the MD simulation for these alloys and suggesting further that our interatomic potential is suitable for additional simulations of mechanical properties of Cu-Zr metallic glasses.

II. EXPERIMENTAL STUDY

A. Synthesis

Cu_xZr_{100-x} $(33.3 \leq x \leq 64.5)$ alloys were prepared by arc-melting buttons of high-purity Cu and Zr; buttons were remelted several times to increase chemical uniformity. After arc-melting, the buttons were melted again and cast into a 10-mm-diam Cu mold. Approximately 15 g of a cast ingot was cut and used to prepare ribbons by single-roller Cu wheel melt spinning at a linear surface velocity of 25 ms^{-1}. Graphite nozzles were used to prevent additional O contamination that frequently occurs when SiO_2 is used.[24] For each Cu_xZr_{100-x} composition, a superheat of approximately 70 K was used prior to ejecting the liquid onto the rotating Cu wheel. The O contents of the melt spun ribbon, as determined by inert gas fusion, were all below 200 ppmw.

B. Diffraction study

The amorphous structure of the melt spun ribbons was confirmed using high-energy x-ray diffraction (HEXRD) at the 6-ID-D MUCAT beam line of the Advanced Photon Source at Argonne National Laboratory. A beam energy of 100 keV ($\lambda = 0.012\,466\,5$ nm) was utilized for the experiments, which were performed in a transmission geometry. For these studies, the volume of material exposed to the 0.3×0.3 mm photon beam was approximately 0.1 mm^3. A MAR 345 digital image plate with a 100×100 μm pixel size was positioned ~300 mm behind the samples to record the two-dimensional scattering pattern over a Q range up to 25 $Å^{-1}$, where Q is the wave momentum transfer number ($Q = 4\pi \sin\theta/\lambda$). The camera length and beam center were determined by fitting the pattern from NIST Si-standard 640C using the FIT2D software.[25]

After correcting for absorption, polarization, multiple scattering, and Compton scattering,[26] the total structure factor, $S(Q)$, was calculated according to

$$S(Q) = 1 + \left(I^e(Q) - \sum_{i=1}^{n} a_i |f_i(Q)|^2 \right) \Bigg/ \left| \sum_{i=1}^{n} a_i f_i(Q) \right|^2, \tag{1}$$

where $I^e(Q)$ is the elastically scattered photons, a_i is the atomic proportion, and $f_i(Q)$ is the Q-dependent scattering factor for each component. Figure 1 shows the total structure factors (TSF) for the glasses with the smallest and largest Cu concentrations used in the present study.

C. Measurement of acoustic velocity

Young's modulus, E, can be experimentally determined from a measurement of the acoustic velocity, v, in combination with the material density, ρ (expressed in kg/m^3):

$$E = \rho v^2. \tag{2}$$

This method allows calculation of a modulus value from a single velocity measurement provided that an extensional wave is used in a bounded media. In order to obtain accurate velocity values without necessitating correction using Poisson's ratio, it is important that the largest dimension of the sample transverse to the wave propagation direction be much less than the wavelength of the acoustic wave used. This limitation makes the velocity measurement in melt spun ribbon attractive, especially since the melt spin process allows forming ribbons with smooth sides, thereby minimizing internal reflections within the ribbon.

A sample holder was designed to allow a length of ribbon to be suspended between two acoustic transducers, the

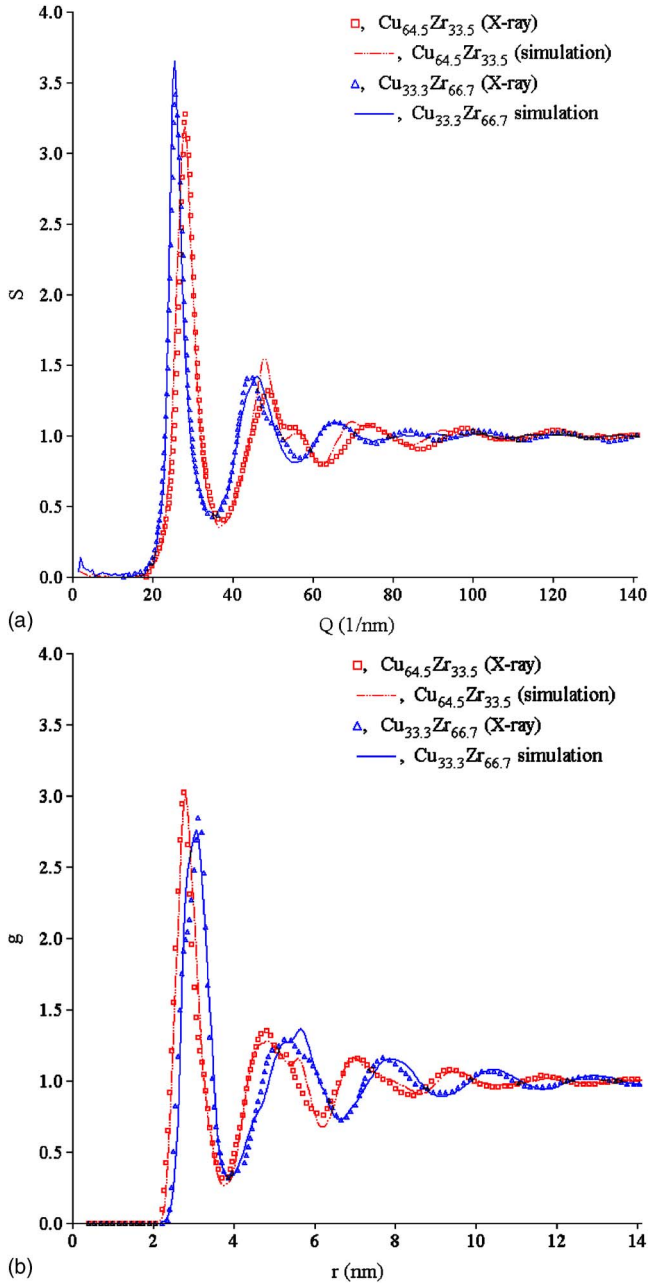

FIG. 1. (Color online) (a) Total structure factors and (b) total pair correlation functions of $Cu_{64.5}Zr_{35.5}$ and $Cu_{33.3}Zr_{66.7}$ metallic glasses from experiment and simulation.

first for introduction of the wave into the ribbon and the second for reception. The sample holder was designed for measurements to be made over two lengths of ribbon with a known distance change. A measurement of the difference in arrival time for the change in ribbon length was accomplished using storage of the acoustic waves for the two ribbon lengths with a Lecroy WaveRunner digital oscilloscope. The difference in arrival time combined with a known distance change allows a straightforward calculation of the velocity and thus the modulus.

A calculation of the wavelength based on the velocity results from these experiments together with the 500 kHz generated frequency yields a wavelength of approximately 1.5 cm. Since the ribbons being examined have cross-sectional dimensions of approximately 1.5 mm by 0.02 mm, the condition that the largest of these dimensions be much less than the wavelength is easily satisfied.

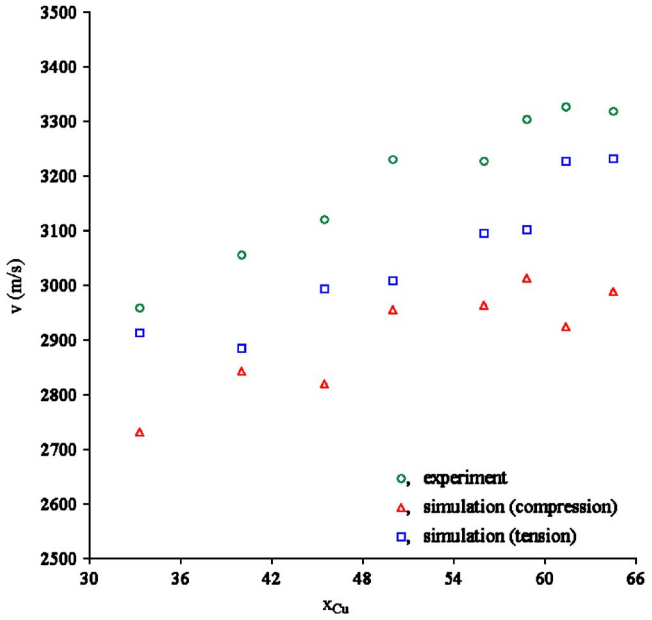

FIG. 2. (Color online) Sound velocity as a function of Cu concentration determined from experiment and simulation.

Figure 2 shows that the measured acoustic velocity clearly rises with increasing Cu concentration. Partially, this rise is related to the fact that the density decreases with increasing the Cu concentration (see Sec. III A). However, the variation of the density in the Cu_xZr_{100-x} $(33.3 \leq x \leq 64.5)$ concentration range is only 10%, while the variation in v^2 is 26%. Therefore, we conclude that Young's modulus increases with increasing Cu concentration.

III. COMPUTER SIMULATION

A. Creation of metallic glass models

In the present study, we performed MD simulations at $T=300$ K using the Cu-Zr interatomic potential developed in Ref. 23 to determine the elastic properties of the Cu-Zr metallic glasses. This particular interatomic potential is of the Finnis-Sinclair (FS) type. While the detailed description of the potential can be found in Ref. 23, we provide brief information about this potential relevant to the present study. The Cu-Zr potential consists of two FS potentials for pure metals that were fitted to the perfect crystal properties and crystal defect properties at $T=0$, melting temperature data, and the liquid structure factors (see Refs. 27 and 28 for details). This combination makes these potentials an excellent choice for simulating the structure and properties of metallic glasses. However, the FS potential for alloys also contains two cross functions. These functions were fitted in Ref. 23 to the lattice constants and formation energies of several metastable Cu-Zr compounds (the data were obtained from the first-principles calculations). Note that no elastic constant or liquid structure data for alloys were used in the fitting pro-

TABLE I. The approximation formulas for the atomic volume as a function of Cu concentration.

x_{Cu}	V (T) (Å^3/at)
0.333	$19.249289416300+1.1177599167666\times10^{-3}$ T $-4.5661594333317\times10^{-8}$ T^2
0.400	$19.035287817541+4.3835848313515\times10^{-4}$ T $+1.4582949464712\times10^{-7}$ T^2
0.455	$18.380328464235+3.9945499740900\times10^{-4}$ T $+1.6346157491169\times10^{-7}$ T^2
0.500	$17.839721065659+3.8602639274784\times10^{-4}$ T $+1.6912231018636\times10^{-7}$ T^2
0.560	$17.131065156300+3.2132069205011\times10^{-4}$ T $+1.9762944649995\times10^{-7}$ T^2
0.588	$16.806545331735+2.6619761699213\times10^{-4}$ T $+2.2528660074511\times10^{-7}$ T^2
0.614	$16.494408408523+2.5725809413933\times10^{-4}$ T $+2.3011521927446\times10^{-7}$ T^2
0.645	$16.161255899500+2.0310168848328\times10^{-4}$ T $+2.5099688603336\times10^{-7}$ T^2

cedure. Therefore, the applicability of these potentials to the simulation of the structure and mechanical properties of the Cu-Zr alloys must be verified.

To obtain glass models at $T=300$ K, we first created a 25 000-atom liquid model at $T=2000$ K. In order to determine the equilibrium density, three models for each Cu concentration were created using NVT molecular dynamics at three densities and the equilibrium density was determined as the one in which the $p(V)$ curve crosses zero. Next the equilibrium models were momentarily cooled down to $T=1500$ K and the procedure to determine the equilibrium density was repeated. Finally, these $T=1500$ K equilibrium models were quenched to $T=0$ and the corresponding equilibrium density was determined. The overall procedure allowed us to obtain the first approximation for the atomic volume as a function of temperature for each Cu concentration. These approximation formulas are given in Table I.

The equilibrium liquid models at $T=2000$ K were cooled down to 300 K at a cooling rate of 4.9×10^{11} K/s. At each MD step, the atomic density was changed according to appropriate approximation formulas. If the employed atomic volume formulas were exact and the cooling velocity was very slow, then the pressure would be zero during the entire cooling process (provided that no phase transformations occur). The actual variation of pressure as a function of the model temperature is shown in Fig. 3. The fact that pressure becomes negative below $T=1500$ K simply reflects the fact that we used rather rough approximations for the atomic density. The curves for all alloys except for $Cu_{33.3}Zr_{66.7}$ look more or less the same, and it is not clear what causes the anomalous behavior for this composition. As discussed below, the $Cu_{33.3}Zr_{66.7}$ model does not exhibit any other special features.

The models obtained by cooling down to $T=300$ K were relaxed by NVT MD during 40 ps and then the pressure was averaged over the next 40 ps. This procedure was repeated for several densities for each composition to determine the equilibrium density. Figure 4 shows the pressure as a function of hydrostatic strain for the two limiting compositions used in the present work. The fact that pressure is almost a linear function of the hydrostatic strain demonstrates that at least metastable states were reached in these models. The equilibrium atomic volume as a function of the Cu concentration is shown in Fig. 5. The atomic volume decreases with increasing Cu concentration, which is obviously related to the fact that Cu atoms have a smaller atomic radius than the Zr atoms.

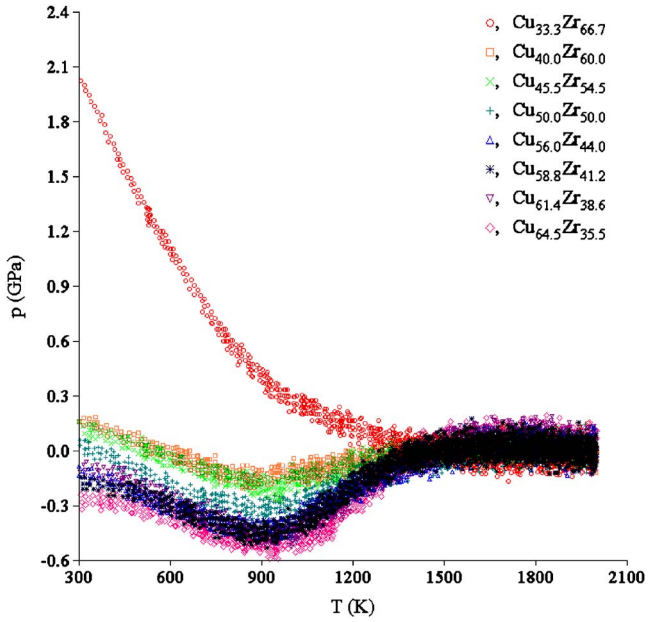

FIG. 3. (Color online) Variation of pressure during cooling of simulated liquid structures.

Figure 1 shows the x-ray TSFs calculated from created models discussed above in comparison with the experimental data. Taking into account that the data from the diffraction experiments were not used in the potential development pro-

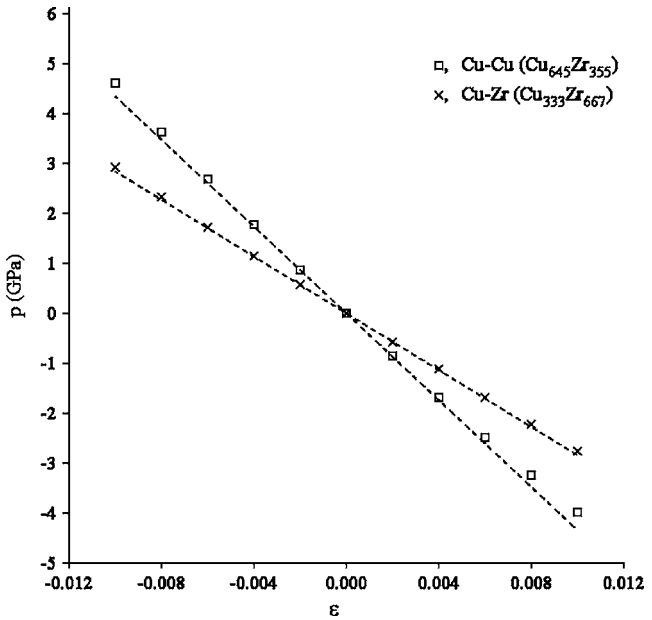

FIG. 4. Pressure as a function of hydrostatic strain. The dashed straight lines are calculated using bulk moduli determined from simulated glass structures.

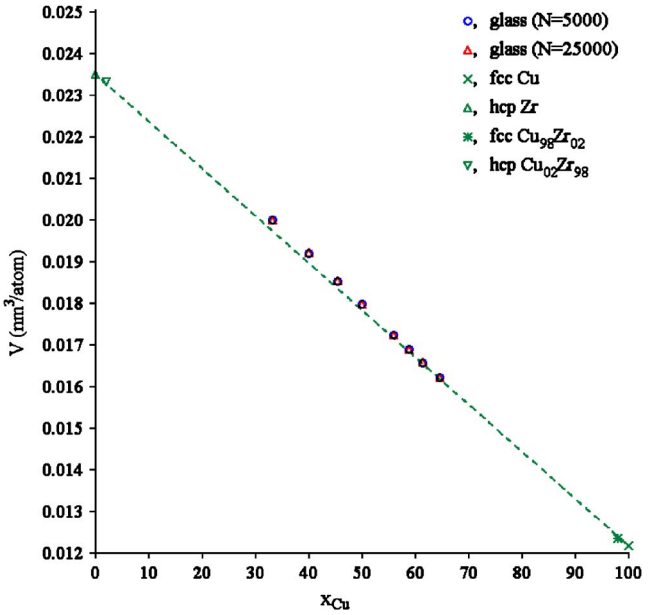

FIG. 5. (Color online) Atomic volume as a function of Cu concentration. All data are from simulations performed in the present work. The dashed straight line connects the values for pure crystalline Cu and Zr.

cedure in Ref. 23, the obtained agreement should be considered as good. However, it should be noted that, in part, this good agreement is related to the fact that the semiempirical potentials for pure elements developed in Refs. 27 and 28 were fitted to experimental diffraction data obtained from elemental Cu and Zr liquids using a similar experimental setup.

The bulk modulus, B, can be calculated from the dependence of pressure on the atomic volume. The results are shown in Fig. 6. This figure clearly demonstrates that the bulk modulus increases with increasing Cu concentration.

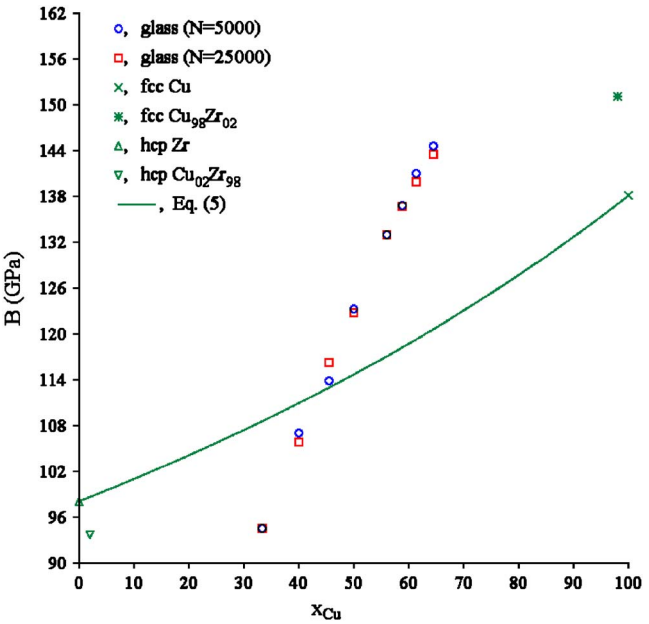

FIG. 6. (Color online) Bulk modulus as a function of Cu concentration. All data are from simulations performed in the present work. The line is from empirical expression from Ref. 30 discussed in Sec. IV.

Note that the employed potentials predict at room temperature the following values of the bulk modulus for pure components: 138.1 and 98.1 GPa (the experimental values are 137.1 and 95.4 GPa, respectively[29]). Thus it is not surprising that the addition of Cu increases the bulk modulus. However, the amorphous alloys with Cu concentrations of 0.614 and 0.645 have a bulk modulus higher than pure crystalline Cu, while the amorphous alloy with a Cu concentration of 0.333 has a bulk modulus smaller than for pure Zr. Thus it appears that the addition of Zr to pure Cu increases the bulk modulus while the addition of Cu to pure Zr decreases the bulk modulus. Unfortunately, we have no experimental data to test this assumption. Therefore, we created models of random solid solutions of Zr in fcc Cu and Cu in hcp Zr at $T=300$ K with solute concentration of 2%. The calculated bulk moduli are shown in Fig. 6 and indeed show that the addition of Cu to pure Zr decreases the bulk modulus, while the addition of Zr to pure Cu increases the bulk modulus.

In order to check whether our models were sufficiently large, we repeated all procedures described above for $N=5000$. The obtained densities and bulk moduli are shown in Figs. 5 and 6, respectively. The analysis of these figures shows no systematic errors associated with the model size.

B. Determination of the elastic constants related to shear deformation

The bulk modulus is necessary to describe the hydrostatic deformation, but it is not sufficient to describe any deformation involving shear. In order to obtain Young's modulus from our simulated models, we applied uniaxial strain in the z direction, ε_{zz}, while the model size in the x and y directions was kept fixed. The model was relaxed during 40 ps and then the normal component of the stress tensor in the z direction, σ_{zz}, was averaged over the next 40 ps. Young's modulus can be calculated via the following expression:

$$E = 9B\frac{\sigma_{zz} - B\varepsilon_{zz}}{\sigma_{zz} + 3B\varepsilon_{zz}}. \tag{3}$$

It should be noted that, on the one hand, Eq. (3) is valid in the linear elasticity regime and, therefore, its accuracy increases as the applied strain approaches zero. On the other hand, if the applied strain is too small, then the average stress will be smaller than the stress fluctuations associated with the finite model size (~0.02 GPa at $T=300$ K). Accordingly, we used 0.5% strain in order to determine Young's modulus. The series of MD simulations were performed with both compressive and tensile strains. The determined value of σ_{zz} varied in the limits from 0.45 to 0.72 GPa. Since it is easy to write equations analogous to Eq. (3) when the model is strained in the x or y directions, we also performed corresponding MD simulations such that the values of Young's modulus were averaged over three directions. The obtained results are shown in Fig. 7. First we note that the values for the tensile strain are systematically higher than those for the compressive strain. This means that the strain employed was sufficiently large to raise deviations from linearity elasticity. To characterize the deviations from linear elasticity, we can

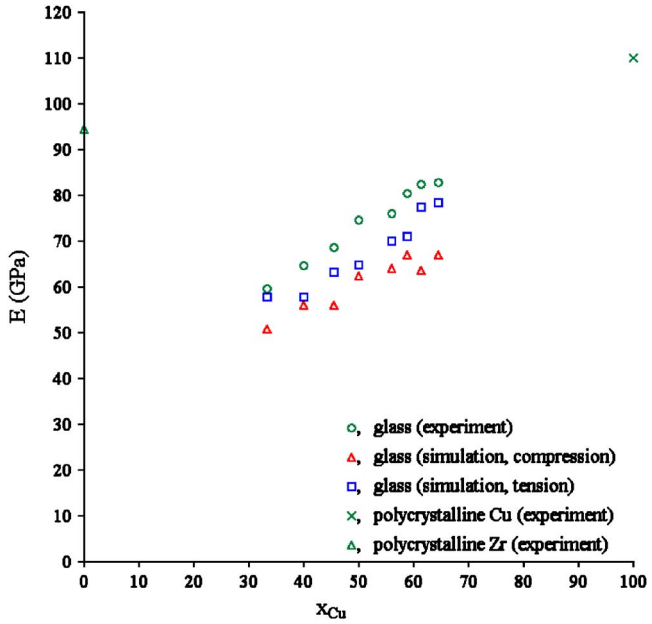

FIG. 7. (Color online) Young's modulus as a function of Cu concentration.

calculate the value of $p+3B\varepsilon$ from the data for the hydrostatic deformation shown in Fig. 4 [note that $p=-(\sigma_{xx}+\sigma_{yy}+\sigma_{zz})/3$ and $\varepsilon=\varepsilon_{xx}=\varepsilon_{yy}=\varepsilon_{zz}$]. In the case of linear elasticity, $p+3B\varepsilon$ should be zero. Figure 8 shows this quantity calculated from the data presented in Fig. 4 and illustrates that at the same applied strain, the deviations from linearity increase with increasing Cu concentration, which is reasonable since the stiffness of the alloys also increases with increasing Cu concentration. While the noise in the data shown in Fig. 7 does not allow us to make a final conclusion, it looks like there is a trend toward increasing the difference between the values of Young's modulus obtained in the tension and compression series with an increase of Cu concentration.

Since both the atomic volume and Young's modulus were determined from computer simulation, we calculated

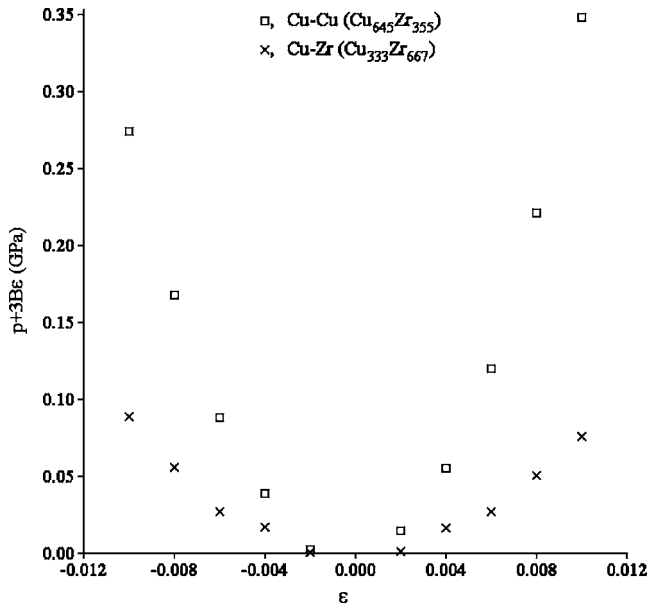

FIG. 8. Deviation from linear elasticity as a function of applied strain.

the acoustic velocities using Eq. (2). The results are shown in Fig. 2 in comparison with the experimental data. Taking into account that the elastic properties of the alloys were not used in the potential development procedure in Ref. 23, the obtained agreement should be considered as good. This agreement demonstrates that the employed potential is suitable for the simulation of certain mechanical properties in Cu-Zr metallic glasses.

Young's modulus can also be calculated via Eq. (2) using the experimental data on the acoustic velocity and the atomic density determined from the computer simulation. Since the experimental inaccuracy of the determination of the acoustic velocity is less than 1% and the inaccuracy in the atomic density cannot exceed 2%–3%, the accuracy of the obtained Young's moduli should be no worse than 3%–4%. The results are shown in Fig. 7. Analysis of this figure shows that the simulation underestimates Young's modulus, but predicts the correct trend for its dependence on the Cu concentration. It is interesting to note that the value of Young's modulus for polycrystalline Cu follows the same trend as obtained for the amorphous alloy. However, the value of Young's modulus for polycrystalline Zr is much higher than expected based on the same trend. Obviously the concentration dependence of Young's modulus for smaller Cu concentration should be more complicated than that in the concentration range examined in the current study; this issue deserves further consideration.

The model glass systems were used to determine additional elastic constants as a function of composition. The Poisson ratio can be calculated as

$$\nu = \frac{3B - E}{6B} \tag{4}$$

and the shear modulus can be calculated as

$$\mu = \frac{E}{2(1+\nu)}. \tag{5}$$

The simulation results are shown in Figs. 9 and 10, respectively. Similar to the predictions of Young's modulus, both the Poisson ratio and the shear modulus increase with increasing Cu concentration.

IV. DISCUSSION AND CONCLUSIONS

In the present work, we employed the semiempirical interatomic potential developed in Ref. 23 to calculate the elastic constants of the Cu-Zr metallic glasses. Using these elastic constants, we calculated the acoustic velocity, which can be directly compared with experimental measurements. This comparison showed that while the employed potential underestimates the acoustic velocity, it correctly predicts the concentration dependence of this quantity. Since the difference between simulation and experimental data is only about 10% (the tension series), we believe that this potential can be used to simulate other mechanical properties and deformation behavior of Cu-Zr metallic glasses.

Analysis of the simulation data shows that all elastic constants (B, E, ν, and μ) increase with increasing Cu concentration. However, the extrapolations of the obtained de-

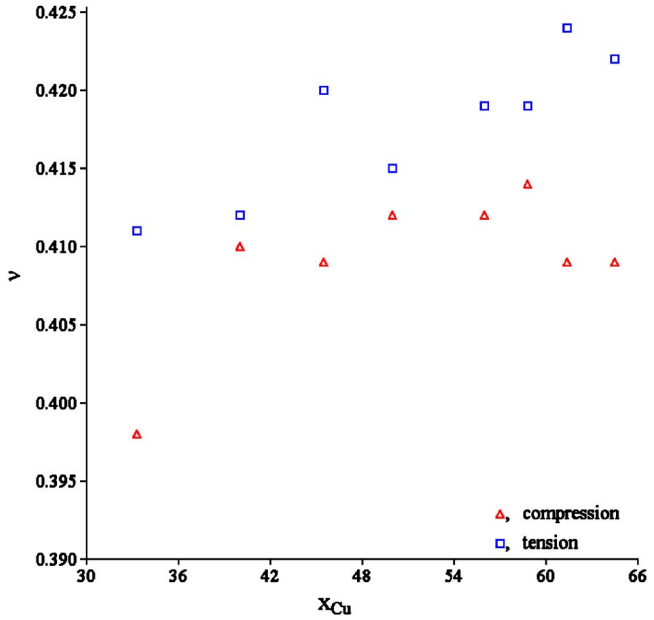

FIG. 9. (Color online) Poisson's ratio as a function of Cu concentration. All data are from simulations performed in the present work.

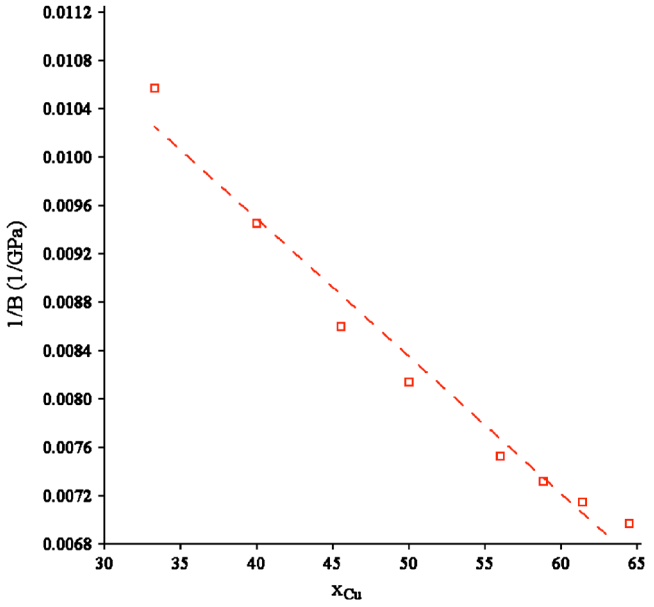

FIG. 11. (Color online) Testing Eq. (6) discussed in the text using bulk moduli determined from simulations performed in the present study. The dashed line represents the best linear fit.

pendences for the bulk modulus and Young's modulus to pure components would provide wrong predictions, as can be seen, in particular, in Figs. 6 and 7. Zhang *et al.* in Ref. 30 proposed the following simple equation to estimate any elastic constant, M, of metallic glasses:

$$\frac{1}{M} = \frac{1 - x_2}{M_1} + \frac{x_2}{M_2}, \tag{6}$$

where M_i are the elastic properties of pure elements. Since pure elements usually cannot be obtained in the amorphous state, the data for pure crystalline metals were used instead in Ref. 30. Since this equation is supposedly valid for any metallic glass, we checked whether it is applicable to describe our simulation data. The most accurate data in the present work were obtained for the bulk modulus. The estimation made using Eq. (6) is shown in Fig. 6 and reveals that while Eq. (6) can provide occasionally a good agreement with experiment (e.g., for $x_{Cu}=0.455$ in our case), it is not able to predict the proper concentration dependence. One may wonder whether this failure of Eq. (6) is related to the choice of the state for pure elements. For example, Zr undergoes an hcp-bcc transition at $T=1136$ K. While the bcc phase does not exist at room temperature, it is possible that the structure of a Zr-rich metallic glass obtained by melt spinning may have local atomic coordinations that resemble the bcc Zr. If this is the case, then using the bulk modulus for the hcp Zr in Eq. (6) is not justified. Thus the simplest way to test Eq. (6) is to plot $1/B$ versus Cu concentration, as shown in Fig. 11. According to Eq. (6), the $1/B$ versus Cu concentration dependence should be a straight line, which is in contrast to the relationship depicted in Fig. 11.

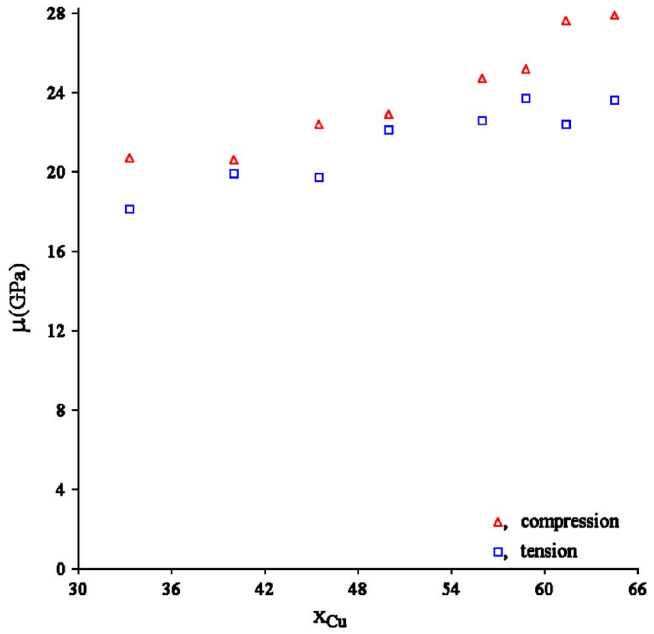

FIG. 10. (Color online) Shear modulus as a function of Cu concentration. All data are from simulation performed in the present work.

The increase in the bulk modulus with increasing Cu concentration can be understood by the examination of Fig. 12, where the changes in the positions of the first peaks of the partial-pair correlation functions (PPCF) as a result of hydrostatic deformation are shown. First, we note that these changes depend very weakly on the Cu concentration. Second, we note that the changes in the Cu-Cu and Cu-Zr PPCFs are rather close to each other, while the position of the first peak of the Zr-Zr PPCF changes by roughly twice as much. Consequently, a decrease in the number of the Zr-Zr nearest neighbors should increase the overall bulk modulus. Since the number of the Zr-Zr nearest neighbors indeed decreases at higher Cu concentrations, the bulk modulus, therefore, increases as well. However, this simple idea does not explain why the same interatomic potential predicts that the

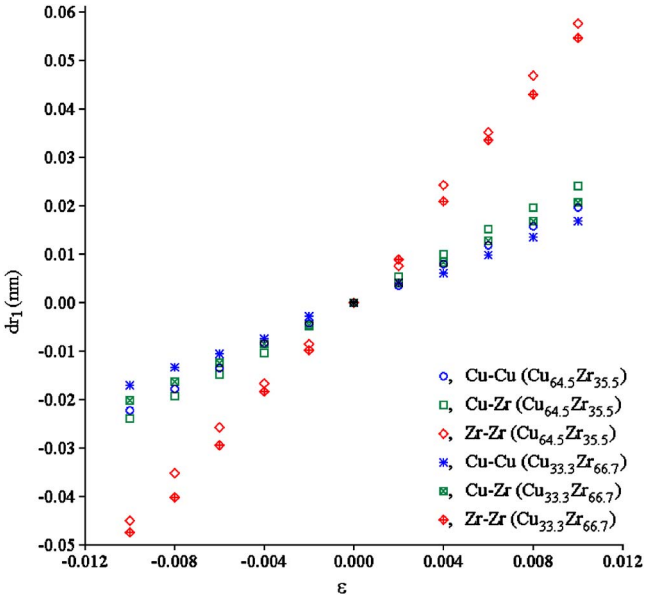

FIG. 12. (Color online) Change in the first-peak positions of PPCFs as a function of imposed hydrostatic deformation.

bulk modulus of fcc Cu increases with the addition of a small amount of Zr or why the bulk modulus of the hcp Zr decreases with the addition of Cu (see Fig. 6).

This study shows that the compositional dependence of elastic constants in metallic glasses can be rather complex even in the case of binary alloys. Further efforts to systematically collect elastic constant data for metallic glasses will help to establish increasingly reliable empirical rules to help design metallic glasses with tailored elastic properties.

ACKNOWLEDGMENTS

Work at the Ames Laboratory was supported by the U.S. Department of Energy, Office of Basic Energy Sciences, under Contract No. DE-AC02-07CH11358. The high-energy x-ray work at the MUCAT sector of the APS was supported by the U.S. Department of Energy, Office of Science, Basic Energy Sciences under Contract No. DE-AC02-06CH11357.

[1] M. L. Lind, G. Duan, and W. L. Johnson, Phys. Rev. Lett. **97**, 015501 (2006).
[2] A. P. Sokolov, V. N. Novikov, and A. Kisliuk, Philos. Mag. **87**, 613 (2007).
[3] J. J. Lewandowski, W. H. Wang, and A. L. Greer, Philos. Mag. Lett. **85**, 77 (2005).
[4] G. J. Fan, M. Freels, H. Choo, P. K. Liaw, J. J. Z. Li, W. K. Rhim, W. L. Johnson, P. Yu, and W. H. Wang, Appl. Phys. Lett. **89**, 241917 (2006).
[5] J. Schroers and W. L. Johnson, Phys. Rev. Lett. **93**, 255506 (2004).
[6] W. H. Wang, J. Appl. Phys. **99**, 093506 (2006).
[7] N. P. Kobelev, E. L. Kolyvanov, and V. A. Khonik, Solid State Phenom. **115**, 113 (2006).
[8] P. Wen, G. P. Johari, R. J. Wang, and W. H. Wang, Phys. Rev. B **73**, 224203 (2006).
[9] M. Hojo and H. Numakura, Mater. Sci. Eng., A **442**, 268 (2006).
[10] T. Rouxel, C. R. Mec. **334**, 743 (2006).
[11] W. H. Wang, C. Dong, and C. H. Shek, Mater. Sci. Eng. **44**, 45 (2004).
[12] R. L. McGreevy, J. Phys.: Condens. Matter **13**, R877 (2001).
[13] M. I. Mendelev, Physica B **262**, 40 (1999).
[14] A. K. Soper, Phys. Rev. B **72**, 104204 (2005).
[15] G. C. Rutledge, Phys. Rev. E **63**, 021111 (2001).
[16] T. Tomida and T. Egami, Phys. Rev. B **48**, 3048 (1993).
[17] Y. Shi and M. L. Falk, Phys. Rev. Lett. **95**, 095502 (2005).
[18] M. Wakeda, Y. Shibutani, S. Ogata, and J. Park, Intermetallics **15**, 139 (2007).
[19] G. Duan, D. Xu, Q. Zhang, G. Zhang, T. Cagin, W. L. Johnson, and W. A. Goddard, Phys. Rev. B **71**, 224208 (2005).
[20] S. Ogata, F. Shimizu, J. Li, M. Wakeda, and Y. Shibutani, Intermetallics **14**, 1033 (2006).
[21] M. S. Daw and M. I. Baskes, Phys. Rev. B **29**, 6443 (1984).
[22] M. W. Finnis and J. E. Sinclair, Philos. Mag. A **50**, 45 (1984).
[23] M. I. Mendelev, D. J. Sordelet, and M. J. Kramer, J. Appl. Phys. **102**, 043501 (2007).
[24] M. H. Lee, R. T. Ott, M. F. Besser, M. J. Kramer, and D. J. Sordelet, Scr. Mater. **55**, 505 (2006).
[25] A. P. Hammersley, S. O. Svensson, M. Hanfland, A. N. Fitch, and D. Hausermann, High Press. Res. **14**, 235 (1996).
[26] X. Qiu, J. W. Thompson, and S. J. L. Billinge, J. Appl. Crystallogr. **37**, 678 (2004).
[27] M. I. Mendelev and G. J. Ackland, Philos. Mag. Lett. **87**, 349 (2007).
[28] M. I. Mendelev, M. J. Kramer, C. A. Becker and M. Asta, Philosophical Magazine (submitted).
[29] G. Simmons and H. Wang, *Single Crystal Elastic Constants and Calculated Aggregate Properties: A Handbook* (The MIT Press, Cambridge, MA, 1971).
[30] Z. Zhang, R. J. Wang, L. Xia, B. C. Wei, D. Q. Zhao, M. X. Pan, and W. H. Wang, J. Phys.: Condens. Matter **15**, 4503 (2003).